Tree Physiology 27, 115–131

Changes in net ecosystem productivity with forest age following clearcutting of a coastal Douglas-fir forest: testing a mathematical model with eddy covariance measurements along a forest chronosequence

R. F. GRANT,[1,4] T. A. BLACK,[2] E. R. HUMPHREYS[3] and K. MORGENSTERN[2]

[1] *Department of Renewable Resources, University of Alberta, Edmonton, AB T6G 2E3, Canada*

[2] *Faculty of Agricultural Sciences, University of British Columbia, Vancouver, BC V6T 1Z4, Canada*

[3] *Department of Geography, Trent University, Peterborough, ON, Canada*

[4] *Corresponding author (Robert.Grant@afhe.ualberta.ca)*

Received June 8, 2005; accepted December 19, 2005; published online October 2, 2006

Summary We hypothesized that changes in net ecosystem productivity (NEP) during aging of coastal Douglas-fir (*Pseudotsuga menziesii* Mirb. Franco) stands could be explained by (1) changing nutrient uptake caused by different time scales for decomposition of fine, non-woody and coarse woody litter left after harvesting, (2) declines in canopy water status with lengthening of the water uptake pathway during bole and branch growth, and (3) increases in the ratio of autotrophic respiration (R_a) to gross primary productivity (GPP) with phytomass accumulation. These hypotheses were implemented and tested in the mathematical model *ecosys* against eddy covariance (EC) measurements of forest CO_2 and energy exchange in a post-clearcut Douglas-fir chronosequence. Hypothesis 1 explained how (a) an initial rise in GPP observed during the first 3 years after clearcutting could be caused by nutrient mineralization from rapid decomposition of fine, non-woody litter with lower C:N ratios (assart effect), (b) a slower rise in GPP during the next 20 years could be caused by immobilization during later decomposition of coarse woody litter, and (c) a rapid rise in GPP between 20 and 40 years after clearcutting could be caused by nutrient mineralization with further decomposition of coarse woody litter and of its decomposition products. During periods (a) and (b), heterotrophic respiration (R_h) from decomposition of fine and coarse litter greatly exceeded net primary productivity ($NPP = GPP - R_a$) so that Douglas-fir stands were large sources of CO_2. During period (c), NPP exceeded R_h so that these stands became large sinks for CO_2. Hypothesis 2 explained how declines in NPP during later growth in period (c) could be caused by lower hydraulic conductances in taller trees that would force lower canopy water potentials and hence greater sensitivity of stomatal conductances and CO_2 uptake to vapor pressure deficits. Enhanced sensitivity to vapor pressure deficits was also apparent in the EC measurements over the post-clearcut chronosequence. Hypothesis 3 did not contribute to the explanation of forest age effects on NEP.

Keywords: autotrophic respiration, ecosys, GPP, heterotrophic respiration, hydraulic conductance, litter decomposition, NEP, nutrient mineralization, Pseudotsuga menziesii.

Introduction

Many forest ecosystems lose more C from heterotrophic and autotrophic respiration (R_h and R_a) than they gain from CO_2 fixation (= gross primary productivity GPP) for several years after a stand-replacing disturbance (Amiro 2001, Pypker and Fredeen 2002*a*, 2002*b*, Rannik et al. 2002, Kowalski et al. 2003). During this period, C losses are accelerated by the decomposition of forest residue as a result of higher temperatures at the exposed ground surface, while C gains are limited by the low leaf area index (LAI). This period of net C loss (when net ecosystem productivity ($NEP = GPP - R_a - R_h$) is negative) may continue for 10 years or longer in Canadian forests (Kurz and Apps 1999, Litvak et al. 2003), for at least 14 years in Siberian pine forests (Schulze et al. 1999), and for 14 (Janisch and Harmon 2002) or 20 (Cohen et al. 1996) years in coniferous forests of the Pacific Northwest. The GPP rises gradually as forest LAI recovers, whereas R_h declines as residue remaining from the previous forest is depleted, so that the forest eventually starts to regain C (NEP becomes positive). Net primary productivity ($NPP = GPP - R_a$) reaches a maximum about 20–40 years after disturbance (Amiro et al. 1999, Song and Woodcock 2003), but rising R_a with phytomass growth causes NPP to decline gradually thereafter (Mäkelä and Valentine 2001). Over time, litterfall and hence R_h rise, so that a maximum NPP is reached and then NEP gradually declines with advancing age (Litvak et al. 2003).

Here, three hypotheses about why forest productivity changes with age are considered. According to Hypothesis 1, during the first few years after disturbance, the rapid decomposition of fine plant litter with comparatively low C:nutrient

ratios can cause a transient net mineralization of nutrients that may stimulate early regeneration of LAI and a rise in GPP, mostly from herbaceous pioneer species (assart effect; Kimmins 2004). However the slower decomposition of large amounts of coarse woody debris with high C:nutrient ratios immobilizes soil nutrients (Schimel and Firestone 1989), causing declines in soil and foliar N concentrations (Bradley et al. 2002), thus constraining nutrient uptake and hence GPP (Kimmins 2004). This constraint is eventually relieved as the coarse woody debris is transformed to products with lower C:nutrient ratios, allowing LAI and GPP to continue rising, mostly through the growth of dominant tree species. Hypothesis 2 predicts that, during subsequent regrowth, as trees become taller, the increased path length for water uptake necessitates lower canopy water potentials (Ψ_c) to maintain transpiration because (a) the gravitational potential difference between soil and canopy increases, and (b) axial hydraulic conductance between soil and canopy declines (Hubbard et al. 1999), although these declines may be partially offset by increases in sapwood area (Becker et al. 2000). Lower Ψ_c can reduce stomatal conductance (g_c) and hence GPP, without reducing the maintenance component (R_m) of R_a, so that R_a:GPP rises and NPP declines. Hypothesis 3 predicts that, during regrowth, as trees become larger, the ratio of R_m to GPP increases, thereby lowering NPP (Cannell 1989); however, once maximum LAI is reached, most phytomass growth is sapwood, the R_m of which may be insufficient to explain observed declines in NPP with age (Ryan and Waring 1992).

Because forest age strongly affects net ecosystem production (NEP), there is a need to estimate the time course of NEP following disturbance as part of national projections of forest C inventories under different disturbance regimes. These estimates have relied on the use of mathematical models in which age effects on GPP are usually based on growth curves (Li et al. 2002, Peng et al. 2002) or allometric relationships (Song and Woodcock 2003) of different forest types derived from existing inventories of wood volume. In these models, R_a is commonly assumed to be a set fraction of GPP, and R_h is driven by first-order functions of litter and soil C pools. These modeled effects require assumptions about the time course and limits of forest growth that may not be valid under site conditions and climates differing from those under which the models were developed. A more robust approach to modeling age effects on forest productivity is explicit simulation of the processes underlying the hypotheses outlined. In this study, we tested whether these processes, as simulated in the ecosystem model *ecosys* (Grant 2001), can explain changes in hourly CO_2 and energy exchange and annual NEP measured in Douglas-fir stands of different ages following clearcutting in coastal British Columbia (Humphreys et al. 2005, Morgenstern et al. 2004). We then used the model to project changes in net biome productivity (NBP = NEP – C removals from disturbance) caused by different practices of stand regeneration (suppression of pioneer vegetation, removal of surface residue) and harvesting (60-year versus 120-year logging cycles).

Model development

A comprehensive description of *ecosys* has been presented (Grant 2001). Descriptions of those parts of the model relevant to the three hypotheses for forest age effects on NEP are provided here with reference to the equations and variables presented in supplementary tables posted on the web (Appendix 1). The values of all variables that function as input parameters are the same as those used in the earlier publications cited in Appendix 1 and in the descriptions below.

Plant litter transformations (Hypothesis 1)

Plant litter decomposition Organic transformations in *ecosys* occur in five organic matter–microbe complexes *i* (coarse woody litter, fine non-woody litter, animal manure, particulate organic matter (POM), and humus) in each soil layer. Each complex consists of five organic states: solid organic matter, dissolved organic matter (including acetate for methanogenesis), sorbed organic matter, microbial biomass and microbial residues, among which C, N and P are transformed. Organic matter in litterfall and manure complexes are partitioned into carbohydrate, protein, cellulose and lignin, each of which differs in vulnerability to hydrolysis by heterotrophic decomposers. Coarse woody and fine non-woody litterfall from different deciduous and coniferous species are partitioned from proximate analysis results in Trofymow et al. (1995). Organic matter in particulate organic matter and humus differ in vulnerability to hydrolysis. Microbial biomasses and microbial residues in all complexes are partitioned into labile and resistant components that differ in vulnerability to hydrolysis.

The rate at which each component of each organic state is hydrolyzed $D_{Si,j,C}$ is a first-order function of the N and P contents in the active biomass of all heterotrophic microbial populations $M_{i,n,a}$ (where n includes obligately aerobic, facultatively anaerobic (denitrifiers), obligately anaerobic (fermenters and acetotrophic methanogens) and non-symbiotic diazotrophic functional types) in each organic matter–microbe complex (Equations A1 and A2). Microbial biomass in *ecosys* is thus an active agent of organic matter transformation rather than a passive organic state as in models that use first-order kinetics. The rate at which each component is hydrolyzed, $S_{i,C}$, is a Monod function of substrate concentration (Equations A3 and A4), calculated from substrate mass and the fraction of this mass colonized by $M_{i,n,a}$. Hydrolytic rates are controlled by soil temperature through an Arrhenius function (Equation A5) and by soil water content through its effect on aqueous microbial concentrations [$M_{i,n,a}$] (Equations A3 and A4) in surface detritus and in a spatially resolved soil profile. Soil temperatures and water contents are calculated from surface energy balances and from heat and water transfer schemes through canopy–snow–residue–soil profiles. Release of N and P from hydrolysis of each component in each complex is determined by its N and P concentrations (Equations 6 and 7) which are determined from those of the plant part from which it originated, less nutrients withdrawn by the plant dur-

ing senescence (Equations C14 and C17). Most non-lignin hydrolysis products are released as dissolved organic C, N and P (DOC, DON, and DOP) that are adsorbed or desorbed according to a power function of their soluble concentrations (Equations A8–A10).

Microbial growth, respiration, and decomposition

Heterotrophic respiration in each soil layer R_h is the sum of that by all heterotrophic microbial populations n in each substrate–microbe complex i (Equation A11). Total R_h for all soil layers drives CO_2 emission from the soil surface. Heterotrophic oxidation rates may be constrained by microbial nutrient concentrations (Equation A12), temperature (Equation 13), DOC (Equation A13) and O_2 (Equation 14). Oxygen uptake $R_{O_2 i,n}$ is driven by C oxidation (Equation A15) and constrained by O_2 diffusivity (Equation A16), so that C oxidation is coupled to O_2 reduction by all aerobic populations according to O_2 availability (Grant et al. 1993*a*, 1993*b*, Grant and Rochette 1994). Carbon oxidation not coupled with O_2 is coupled with the sequential reduction of NO_3^-, NO_2^-, and N_2O by heterotrophic denitrifiers (Grant and Pattey 1999, 2003), and with the reduction of organic C by fermenters and acetotrophic methanogens (Grant 1998*a*, Grant and Roulet 2002). In addition, autotrophic nitrifiers conduct NH_4^+ oxidation and NO_3^- production (Grant 1994) and N_2O evolution (Grant 1995*a*), and autotrophic methanogens and methanotrophs conduct CH_4 production (Grant 1998*a*) and oxidation (Grant 1999).

All microbial populations in the model undergo maintenance respiration $R_{Mi,n,j}$ (Equations A17 and A18) and decomposition $D_{Mi,n,j}$ (Equation A22). Internal retention and recycling of microbial N and P during decomposition (Equation A23) is modeled whenever these nutrients constrain R_h (Equation A12). The R_h in excess of maintenance requirements is used as growth respiration $R_{gi,n}$ (Equation A19), the energy yield ΔG of which determines heterotrophic growth, and hence uptake of DOC (Equation A20), DON and DOP (Equation A21). Changes in microbial biomass arise from differences between uptake of DOC and maintenance + growth respiration + decomposition (Equation A24). During these changes, microbial populations seek to maintain set minimum ratios of biomass C to N or P by mineralizing or immobilizing NH_4^+, NO_3^-, and $H_2PO_4^-$ ($I_{i,n,j,N,P}$ in Equation A25), thereby controlling solution concentrations of inorganic N and P. If $I_{i,n,j,N,P}$ is inadequate to maintain these minimum ratios, then ratios of biomass C to N or P rise, but R_h is constrained by the nutrient present in the lowest concentration with respect to that at the minimum ratio (Equation A12). Non-symbiotic heterotrophic diazotrophs ($n = f$) can also fix aqueous N_2 ($\Phi_{i,n=f,j}$ in Equation A26) if $I_{i,n,j,N}$ is inadequate to maintain set maximum ratios of biomass C to N or P, but at an additional respiration cost ($R_{\Phi i,n=f,j}$ in Equation A27). Changes in microbial N and P (Equation A28) arise from organic N and P uptake ($U_{i,n,N,P}$ in Equation A21) plus inorganic N and P immobilization ($I_{i,n,j,N,P}$ in Equation A25), N_2 fixation ($\Phi_{i,n=f,j}$ in Equation A26), less microbial N and P decomposition ($D_{Mi,n,j,N,P}$ in Equation A23). Labile and resistant components of microbial biomass are used to calculate active microbial biomass $M_{i,n,a}$ (Equation A29), which then drives further oxidation of DOC (Equation A1 and A2).

Humification of products from organic matter decomposition

Products from hydrolysis of lignin $D_{Si,j=lignin}$ in litterfall and manure (Equations A1 and A6) are transferred to the particulate organic matter complex (Equations A30–A33) with some of the products from hydrolysis of protein and carbohydrate according to stoichiometry proposed by Shulten and Schnitzer (1997). Products of microbial decomposition $D_{Mi,n,j}$ (Equations A22 and A23) are partitioned between the humus complex and microbial residues in a ratio F_h that depends on soil clay content (Equations A34 and A35; Grant et al. 1993*a*, 1993*b*). These products have lower C:nutrient ratios than does litterfall.

Root and mycorrhizal nutrient uptake Uptake of N and P (e.g. $U_{NH_4^+ s,z}$ in Equation A36) is calculated by solving for solution concentrations at root and mycorrhizal surfaces $[NH_4^+]_{s,z}$ at which radial transport by mass flow and diffusion from the soil solution to these surfaces (Equation A36a) equals active uptake by the surfaces (Equation A36b). Values for root length and surface areas used in Equation A36 are taken from a root growth model (Grant 1998*b*). $U_{NH_4^+ s,z}$ in Equation A36 competes with I_{i,n,j,NH_4} in Equation A25b for NH_4^+ and $U_{PO_4^- s,z}$ competes with I_{i,n,j,PO_4} for $H_2PO_4^-$.

Previous testing of litter transformations algorithms The ability of Equations A1–A35 to model the time courses of CO_2 evolution and of N immobilization–mineralization, nitrification and denitrification has been tested against measurements of substrate consumption, biomass growth, CO_2 emissions and mineral N concentrations during incubation of different soil amendments under controlled changes in temperature and water content (Grant et al. 1993*a*, 1993*b*, 2003, Grant 1994, 1995*a*, 1998*a*, 1999, Grant and Rochette 1994). The ability of Equation A36 to model rates of N and P uptake and of plant growth under different rates of N and P fertilization has been tested against field measurements of phytomass growth and of phytomass N and P contents under different fertilizer rates (Grant 1991, Grant and Robertson 1997, Grant et al. 2001*b*).

Plant water relations (Hypothesis 2)

Canopy transpiration Canopy energy exchange is calculated from an hourly two-stage convergence solution for the transfer of water and heat through the soil–root–canopy of each plant population (e.g., species or cohort) i. The first stage of this solution requires convergence to a value of canopy temperature T_{ci} at which the first-order closure of the canopy energy balance is achieved. During convergence, latent heat flux between the atmosphere and each population LE_i is controlled by canopy aerodynamic (r_{ai}) and stomatal (r_{ci}) resistances (Equation B1). Two controlling mechanisms are postulated for r_{ci}. (1) A minimum canopy stomatal resistance (r_{cmini}) is calculated that allows a set ratio of intercellular to canopy boundary layer CO_2 concentration (C_{ii}':C_b) to be maintained at leaf CO_2 fixation rates calculated at ambient irradiance, T_{ci}, C_{bi} (Farquhar et

al. 1980) and full canopy hydration (canopy water potential $\psi_{ci} = 0$ MPa) (Equation B2). (2) Ambient canopy stomatal resistance r_{ci} is then calculated by raising r_{cmini} through an exponential function of canopy turgor ψ_{ti} (Equation B3) calculated from ψ_{ci} and canopy osmotic potential $\psi_{\pi i}$ (Equation B4) during convergence for transpiration versus water uptake.

Root and mycorrhizal water uptake The difference between ψ_{ci} adjusted for canopy elevation (Equation B7) and soil water potential ψ_{sl} adjusted for root depth (Equation B8), determines water uptake $U_{i,l,z}$ by root and mycorrhizal surfaces z of each plant population i in each layer l (Equation B6). Potential differences act across hydraulic resistances to radial movement through soil to root and mycorrhizal surfaces $\Omega_{si,l,z}$ (Equation B9), and to radial $\Omega_{ri,l,z}$ (Equation B10) and axial $\Omega_{ai,l,z,x}$ (Equations B11 and B12) movement through roots and mycorrhizae to the canopy in each rooted soil layer. Values of Ω_a for primary and secondary root systems are calculated from numbers of parallel primary and secondary root axes (Equations B11 and B12). The number of the primary root axes in Equation B11 is linked to maximum foliar area, allowing Ω_a to decrease somewhat with tree growth. An explicit term for Ω_a of the bole (the second term in Equation B11) is calculated for each rooted soil layer from bole length, number of primary root axes, and the fraction of total root mass, and is added to Ω_a of the primary root system. Root and mycorrhizal resistances were calculated from Poiseuille's law using root radial and axial resistivities derived by Doussan et al. (1998). These calculations use root radii, lengths and surface areas from a root system submodel driven by shoot-root C transfers and root growth (Grant 1998*b*), and bole radii and lengths from a shoot system submodel driven by within-shoot C transfers and growth using established allometric relationships. Root and bole radii are affected by $\psi_{ri,l,z}$ and ψ_{ci}, respectively, according to their bulk moduli of elasticity based on Perämäki et al. (2001).

Canopy water status After convergence for T_{ci}, the difference between canopy transpiration E_i (Equation B1) and total water uptake U_i (Equation B5) is tested against the difference between canopy water content from the previous hour and that from the current hour. This difference is calculated from the capacitance X_i for each plant population i ($[X_i \partial\psi_{ci}/\partial t$ in Equation B13]) derived from foliar mass and bole sapwood area. The difference between $E_i - U_i$ and $X_i \partial\psi_{ci}/\partial t$ is minimized by adjusting ψ_{ci} used in the next convergence cycle.

Previous tests of plant litter transformation algorithms The ability of Equations B1–B13 to model the response of plant water status to different θ has been tested against field measurements of ψ_c, g_c, LE and root water uptake under different irrigation rates in Grant (1995*b*) and Grant et al. (1995*b*, 1999, 2004).

Gross primary productivity and autotrophic respiration (Hypothesis 3)

Gross primary productivity Canopy GPP is the sum of that for each leaf surface defined by population (species or cohort) i, branch j, node k, layer l, azimuth m, inclination n and exposure (sunlit or shaded) o (Equation C1). Following the convergence solution for ψ_{ci}, *ecosys* solves for the mesophyll gaseous CO_2 concentration $C_{i,j,k,l,m,n,o}$ and its aqueous equivalent $C_{ci,j,k,l,m,n,o}$ at which the diffusion rate of gaseous CO_2 into each leaf surface $V_{gi,j,k,l,m,n,o}$ (Equation C2) equals the CO_2 fixation rate of aqueous CO_2 within each leaf surface $V_{ci,j,k,l,m,n,o}$ (Equation C3).

The CO_2 diffusion rate is calculated from the CO_2 concentration gradient across the stomata driven by canopy boundary layer CO_2 concentration C_b, divided by the stomatal resistance $r_{1i,j,k,l,m,n,o}$ (Equation C4). This resistance is calculated for each leaf surface from its minimum value $r_{lmini,j,k,l,m,n,o}$ (Equation C5) and from turgor potential ψ_{t_i} (Equation B4) calculated during convergence for ψ_{ci}. This minimum resistance is calculated from a potential leaf CO_2 fixation rate $V_c'_{i,j,k,l,m,n,o}$ at full hydration ($\psi_{ci} = 0$) when the mesophyll gaseous CO_2 concentration $C_i'_i$ is a set ratio of C_b. The $V_c'_{i,j,k,l,m,n,o}$ is calculated in the same way as is the actual leaf CO_2 fixation rate $V_{ci,j,k,l,m,n,o}$ (Equation C3), but without non-stomatal effects of ψ_{ci} on CO_2-limited $V_{bi,j,k,l,m,n,o}$ (Equation C6) and irradiance-limited $V_{ji,j,k,l,m,n,o}$ (Equation C7) reaction rates through $f\psi$ (Equation C9). These non-stomatal effects are less constraining to $V_{ci,j,k,l,m,n,o}$ than are stomatal effects to $r_{1i,j,k,l,m,n,o}$ (Equation C4), so that when ψ_{ci} declines below zero, $r_{1i,j,k,l,m,n,o}$ rises above $r_{lmini,j,k,l,m,n,o}$ (Equation C4) and $C_{ii,j,k,l,m,n,o}$ declines below $C_i'_i$ (Equation C2). Leaf stomatal resistance $r_{1i,j,k,l,m,n,o}$ is thus calculated in the same way as is canopy stomatal resistance r_{ci} (Equation B3) (see Canopy transpiration above) but using a leaf level value for V_c'.

The CO_2 fixation rate $V_{ci,j,k,l,m,n,o}$ (Equation C3) is calculated as the minimum of CO_2-limited $V_{bi,j,k,l,m,n,o}$ (Equation C6) and irradiance-limited $V_{ji,j,k,l,m,n,o}$ (Equations C7 and C8) reaction rates according to Farquhar et al. (1980). These rates are constrained by ψ_{ti} (Equation C9), T_{ci} (Equation C10), and by N and P uptake (Equation A36) through their effects on non-structural N and P concentrations $\sigma_{Ni,j}$ and $\sigma_{Pi,j}$ (Equation C11) (Grant 1998*b*). These reaction rates are driven by the products of specific rubisco or chlorophyll activities and areal concentrations ($V_{bmaxi,j,k}$ and $J_{maxi,j,k}$). These concentrations reflect the environmental conditions by which the mass, area, and N and P contents of each leaf were determined during its growth in the model. The photosynthetic photon flux $I_{i,l,m,n,o}$ driving $V_{ji,j,k,l,m,n,o}$ (Equation C8) is calculated for each leaf surface from the cumulative photon flux absorbed by leaves of known optical properties.

Autotrophic respiration and litterfall Autotrophic respiration R_a is the sum of that for all branches j and all root axes z in all soil layers l in each population i (Equation C12). Autotrophic respiration in each plant branch or root axis has two components. The first component $R_{ci,j}$ and $R_{ci,l,z}$ is driven by the first-order oxidation of nonstructural C pools $\sigma_{Ci,j}$ (Equation C13) or $\sigma_{Ci,l,z}$ which are the products of CO_2 fixation (Equation C1) and nonstructural C transfer. This transfer is driven by concentration gradients of $\sigma_{Ci,j}$ that arise from fixation of $\sigma_{Ci,j}$ in shoots versus oxidation of $\sigma_{Ci,j}$ in shoots and

roots. Oxidation is constrained by organ water and nutrient status, which under adverse conditions decline more rapidly in shoots than in roots. Such conditions raise concentration gradients of $\sigma_{Ci,j}$ and favor shoot–root transfer (Grant 1998*b*).

The second component of R_a is driven by the respiration of remobilizable C ($R_{si,j}$ and $R_{si,l,z}$) in leaves and supporting structures or roots to meet maintenance respiration requirements $R_{mi,j}$ or $R_{mi,l,z}$ when these exceed $R_{ci,j}$ or $R_{ci,l,z}$. The $R_{mi,j}$ is calculated independently of $R_{ci,j}$ from the N content in each plant organ *z*, and a function of canopy or root temperature (Equation C15). The N content of wood in Equation C15 includes only that in a shell of set thickness around the circumference of the bole intended to represent sapwood, and so becomes a smaller fraction of total wood N during growth based on the findings of Pruyn et al. (2000).

The $R_{ci,j}$ is first used to meet requirements for $R_{mi,j}$, then any excess is expended as growth respiration $R_{gi,j}$ (Equation C16), which drives the conversion of $\sigma_{Ci,j}$ to phytomass according to organ-specific growth yields $R'_{gi,z}$ (Equation C19). If $R_{ci,j}$ is less than $R_{mi,j}$, $R_{si,j}$ drives the withdrawal of remobilizable N and P (mostly non-structural protein N and P) from leaves and supporting structures into nonstructural N and P reserves, and the loss of associated non-remobilizable C, N and P (mostly structural) as litterfall $L_{i,j}$ (Equation C17). Provision is also made to withdraw remobilizable N or P from leaves and petioles when ratios of $\sigma_{Ni,j}$:$\sigma_{Ci,j}$ or $\sigma_{Pi,j}$:$\sigma_{Ci,j}$ become smaller than those required for phytomass growth, driving the withdrawal of associated remobilizable C, and the loss of associated non-remobilizable C, N and P as litterfall. We modeled R_c, R_m, R_s and L in roots in the same way as in shoots. Environmental constraints such as water, heat or nutrient stress that reduce $\sigma_{Ci,j}$ and hence $R_{ci,j}$ with respect to $R_{mi,j}$ therefore hasten litterfall. Remobilization and litterfall start at the lowest node of each branch at which leaves or petioles are present, and proceed upwards. Phytomass net growth (Equation C19) is driven by $R_{gi,j}$ (Equation C16) less losses from $R_{si,j}$ (Equation C17) and $L_{i,j}$ (Equation C17) in shoots, and by corresponding fluxes in roots. In this modeling approach, R_a is the larger of that driven by GPP (R_c) and by R_m, so that R_a:GPP is not a simple function of phytomass.

Previous testing of algorithms for gross primary productivity and autotrophic respiration The ability of Equations C1–C19 to model the response of plant CO_2 exchange to controlled changes in irradiance, temperature and CO_2 concentration has been tested against measurements of CO_2 flux under laboratory (Grant 1989) and field conditions (Grant et al. 1995*a*, 1999, 2001*b*, 2004) .

Methods

Site description

Three sites with Douglas-fir stands of differing ages but similar soil and weather were selected near the east coast of Vancouver Island, BC, Canada, to provide comparable measurements of forest age effects on CO_2 and energy exchange. The youngest site (the 2000 site) had been in a 32-ha stand of unmanaged ~65 year-old Douglas-fir on a level gravelly fluvial terrace. The stand was clearcut in winter 2000 and planted in spring 2000 with 1-year-old seedlings (93% Douglas-fir and 7% western red cedar) at 1600 ha^{-1} without further management. The next older site (the 1988 site) had been in a 110-ha stand of second-growth Douglas-fir, western red cedar and western hemlock on a 2–5° SE slope. The stand was clearcut in 1987, burned, planted in 1988 with 75% Douglas-fir, 25% western red cedar and 4% grand fir and sprayed with herbicide in 1992. The oldest site (the 1949 site) had been in a 130-ha old-growth stand on a 5–10° NE slope 3 km from the 2000 site and 48 km from the 1988 site. The stand was logged in 1937, and slash-burned in 1943, then allowed to regenerate without further management until a fertilizer application of 20 g N m^{-2} as urea in 1994. Key stand and soil attributes at each site are given in Table 1 and further information is given in Humphreys (2004). These sites were considered similar enough that differences in NEP among them could be attributed largely to differences in forest age.

CO_2 and energy exchange measurements

Carbon dioxide and energy exchange were measured continuously by eddy covariance (EC) over the 2000 site from 2001, over the 1988 site from 2002 and over the 1949 site from 1998 as described by Humphreys et al. (2003). The CO_2 fluxes measured during calm nights when turbulent mixing was inadequate were rejected. We used gap filling techniques to replace these rejected measurements in the calculation of annual exchanges as described by Morgenstern et al. (2004).

Model runs

Ecosys was initialized with the soil and topographic properties given for the 2000 site in Table 1, and with above- and below-ground residues estimated to correspond to those left after logging. The rooting zone consisted of the soil horizons described in Table 1, with subdivision into 11 soil layers to increase spatial resolution. Two additional soil layers with properties the same as those of the lowest rooted layer and with thicknesses of 0.4 and 0.8 m were modeled below the rooting zone. The lower soil boundary was set so that the water content in the lowest soil layer was maintained at field capacity. These additional layers enabled water transfer modeled in the rooting zone to be largely independent of assumptions about drainage through the lower boundary. *Ecosys* was then seeded with Douglas-fir at 0.2 m^{-2} and run for 70 years without further management under repeated 6-year sequences (1998–2003) of weather data recorded at the 1949 site.

After 70 years, a simulated logging was applied in mid-January with removal of 0.1, 0.1 and 0.6 of foliar, non-foliar non-woody, and coarse woody aboveground phytomass, respectively. These fractions allowed the retention of most foliar and non-foliar non-woody C as litterfall, and the removal of 11.5 kg m^{-2} of aboveground coarse woody C as boles, corresponding with observations by Humphreys (2004) after logging of the 2000 site. To simulate disturbance effects on

Table 1. Key stand and soil characteristics in 2002 of three Douglas-fir sites logged in 2000, 1988 and 1949 on the east coast of Vancouver Island, B.C.

Stand characteristic	Year of logging		
	2000	1988	1949
Mean annual temperature	8.3 °C	8.3 °C	8.3 °C
Mean annual precipitation	1461 mm	1461 mm	1461 mm
Elevation (m)	175	170	300
Slope (degree)	0–2	2–5 SE	5–10 NE
Dominant vegetation	Douglas-fir 93% western red cedar 7%	Douglas-fir 75% western red cedar 21%	Douglas-fir 80% western red cedar 17%
Height (m)	0.6	5.8	35
Diameter (m)	0.015	0.075	0.29
Basal area			
Density (ha^{-1})	1500	1240	1100
Understory	Dense: ferns, fireweed, salal, shrubs, asters, thistles, grasses	Dense: ferns, fireweed, salal, shrubs	Sparse
Maximum LAI	2.2[1]	4.5	8.4
Site index	32	29[2]	35
Management	None	None	20 g N m^{-2} as urea in 1994

Soil characteristic[3]	LFH			Ap/Ae			$Bf_1/Bf_2/Bf_c$			C		
	2000	1988	1949	2000	1988	1949	2000	1988	1949	2000	1988	1949
Depth to bottom layer (m)	0.036	0.041	0.030	0.1	0.1	0.1	0.7	0.7	0.7	1.0	1.0	1.0
Bulk density (Mg m^{-3})	0.15	0.15	0.15	1.34	0.84	1.34	1.34	0.84	1.34	1.58	1.58	1.58
Field capacity (m^3 m^{-3})				0.19	0.35	0.21	0.19	0.35	0.21	0.20	0.20	0.20
Wilting point (m^3 m^{-3})				0.05	0.13	0.06	0.05	0.13	0.06	0.07	0.07	0.07
K_{sat} (mm h^{-1})				36	36	36	110	110	110	110	110	110
Sand (g kg^{-1})				692	692	692	856	856	856	879	879	879
Silt (g kg^{-1})				227	227	227	131	131	131	95	95	95
Clay (g kg^{-1})				81	81	81	13	13	13	26	26	26
Coarse fragments (m^3 m^{-3})				0.43	0.29	0.33	0.43	0.29	0.33	0.43	0.29	0.33
pH	5.2	5.2	5.2	5.45	5.45	5.45	5.92	5.92	5.92	6.5	6.5	6.5
Organic C (g kg^{-1})	450	382	385	53	83	74	31	31	31	12	12	12
Total N (g Mg^{-1})	5200	6400	8100	1800	2900	2200	600	600	600	315	315	315

[1] Mostly understory.
[2] The 14-year growth was more consistent with a site index of 35.
[3] From Humphreys (2004).

surface litter, a small fraction (0.05) of surface woody and non-woody litter was incorporated into the soil LFH horizon. All fine non-woody and coarse woody root phytomass was added as litterfall to the soil layers in which they had been growing. The modeled site was then reseeded in mid-March with Douglas-fir at a density of 0.25 m^{-2} and deciduous bush at 0.25 m^{-2} to simulate competing pioneer populations. These two plant populations used common input attributes for cool temperate C_3 perennial species (Tables A2 and A3), and differed primarily in the absence (Douglas-fir) or presence (bush) of seasonally driven senescence and litterfall of aboveground non-woody phytomass. The reseeded site was then run for a further 200 years under repeated 7-year sequences (1998–2004) of weather data recorded at the 2000, 1988 and 1949 sites. During model runs, prescribed thinnings were applied annually to Douglas-fir and deciduous bush populations to reproduce declines in plant populations generally observed during forest regeneration. Urea (20 g N m^{-2}) was added to the surface litter layer during the 45th year of this run to reproduce site management.

Hourly CO_2 and energy fluxes and annual NEP modeled from site weather data were compared with measured half-hourly fluxes and total annual fluxes derived through gap-filling. Comparisons were made during Years 1 to 3 of the model run, corresponding to 2001, 2002 and 2003 at the 2000 site, during Years 14 and 15 of the model run, corresponding to 2002 and 2003 at the 1988 site, and during Years 49 to 54 of the model run, corresponding to 1998 through 2003 at the 1949 site.

Model predictions

To examine changes in modeled NEP in response to various stand regeneration and harvesting practices, the model was re-initialized with the values of all state and driver variables

immediately following the first simulated logging in mid-January 70 years after initial seeding. The modeled site was then reseeded in mid-March, and run with different land use practices under repeated 7-year sequences (1998–2004) of weather data recorded at the 1949 site. In one run, simulated pioneer vegetation was cut at a height of 0.5 m on July 1 of each year to examine sensitivity of modeled stand regeneration to vegetation control. In another run, 0.9, 0.9 and 0.6 of foliar, non-foliar non-woody, and coarse woody aboveground phytomass. respectively, were removed at harvest (versus 0.1, 0.1 and 0.6 in the model test run) to examine sensitivity of modeled stand regeneration to slash removal. In another two runs, simulated forests were harvested after 4 × 60-year and 2 × 120-year logging cycles using the same removal coefficients as those in the model test run to examine sensitivity of modeled stand regeneration to logging frequency.

Results

Plant litter decomposition and plant N uptake

Simulated logging of the initial 70-year-old Douglas-fir stand added 0.7 and 7.7 kg C m^{-2} of fine non-woody and coarse woody litterfall, respectively, to the soil surface, and added 0.4 and 0.3 kg C m^{-2}, respectively, below the soil surface. Although coarse woody litter was not measured after the 2000 clearcut at Campbell River, Janisch and Harmon (2002) calculated mean coarse woody litter of 7.6 kg C m^{-2} (ranging between 4.2 and 11.9 kg C m^{-2}) following clearcutting of Douglas-fir–hemlock forests in the nearby northwestern USA. At the end of the first year after clearcutting, the surface stock of fine non-woody litter in the model declined to 0.70 of its value immediately after clearcutting. A decline to 0.71 in Douglas-fir litter was measured by Trofymow et al. (2002) after 1 year in surface litter bags at Port McNeill in the same ecoclimatic zone on the east coast of Vancouver Island. During the first 3 and 6 years after clearcutting, the surface stock of coarse woody litter in the model declined to 0.85 and 0.67 of its initial value (Equations A1 and A3), similar to declines to 0.86 and 0.71 of initial wood block mass measured by Trofymow et al. (2002) after 3 and 6 years in surface litter bags at Port McNeill.

Following the simulated clearcut, decomposition of fine litter with its comparatively small C:N ratio (about 35:1) released DOC and DON for microbial uptake in the fine litter complex. Uptake of DON enabled net N mineralization from the fine litter complex to begin in the first year after logging. This mineralization caused a brief rise in soil mineral N (NH_4^+ + NO_3^-) (Figure 1a) and in leaching of DON and mineral N (Figure 1b). Mineralization raised plant N uptake, and hence nonstructural N content, causing an early rise in CO_2 fixation (GPP) (Figure 1c), and LAI (Figure 1d), mostly by pioneer bush. The early rise in GPP was consistent with that estimated from EC measurements during the first 4 years after clearcutting at the 2000 site (Table 2).

The decomposition of coarse woody litter with a large C:N ratio (250:1) in the model did not release enough DON for microbial uptake in the coarse woody litter complex, causing immobilization of mineral N and conservation of organic N from the third to the twentieth year after logging. This period in the model is similar to the period during which Chen et al. (2001) found that coarse and fine roots of Douglas-fir retained N during decay after logging (Figure 1a). During this period, microbial populations in *ecosys* conserved N, reducing requirements for external N and allowing heterotrophic activity to be sustained on substrates with large C:N ratios. Immobilization reduced plant N uptake, slowing further gains in modeled GPP (Figure 1c; Table 2) and LAI (Figure 1d).

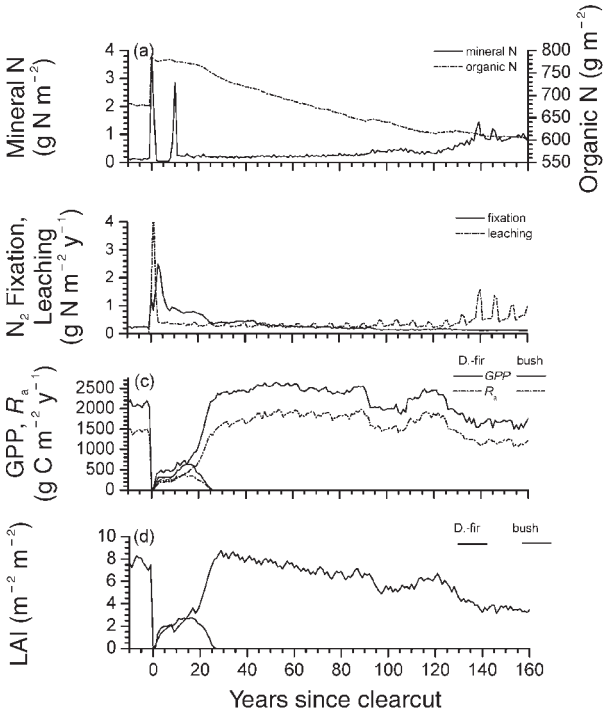

Figure 1. (a) Mineral (NH_4^+ + NO_3^-) and organic N, (b) annual N_2 fixation and N leaching, (c) gross primary productivity (GPP) and autotrophic respiration (R_a), and (d) leaf area index (LAI) modeled during 160 years of Douglas-fir regrowth following clearcutting.

Products of microbial decomposition in the coarse litter complex gradually accumulated in microbial residue pools with lower C:N ratios (Grant et al. 1993*a*, 1993*b*), the decomposition of which eventually generated net N mineralization from the coarse litter complex and hence a decline in organic N starting about 20 years after clearcutting (Figure 1a). Net mineralization raised N uptake and hence GPP (Figure 1c) and LAI (Figure 1d) during the next decade, with maximum values attained about 30 years after clearcutting. During this period, Douglas-fir dominated the deciduous bush, causing its decline. Both GPP and LAI of Douglas-fir declined gradually thereafter.

Non-symbiotic N_2 fixation, driven mostly by N demand from coarse woody litter decomposition, contributed 1–2 g N m^{-2} $year^{-1}$ to microbial N during the first few years after clearcutting (Figure 1b). Fixation declined thereafter, reaching pre-disturbance rates of < 0.5 g m^{-2} $year^{-1}$ after 20 years.

Table 2. Mean annual temperatures (°C) and annual C balances (g C m^{-2}) estimated (E) from site measurements and simulated (S) at Campbell River at different ages following clearcut.

Age	Mean temp.		GPP	R_a	NPP	Litter	Δ Wood	Δ Soil	R_h	R_e	NEP
1–2 (2001)	8.41	E[1]	220							840	−620
		S	151	57	94	18	17	−335	658	715	−564
2–3 (2002)	8.43	E[1]	530							1050	−520
		S	592	256	336	84	31	−754	833	1089	−497
3–4 (2003)	8.91	E[1]	640							1240	−600
		S	759	397	362	178	23	−959	1129	1526	−767
13 (2002)	9.46	E	1210							1340	−130
		S	1275	735	540	414	25	−157	561	1296	−21
49 (1998)	9.10	E[2]	2170							1900	+270
		S	2631	1930	701	305	444	−72	369	2299	+332
50 (1999)	7.64	E[2]	1990							1630	+370
		S	2572	1794	778	273	435	−77	350	2144	+428
51 (2000)	8.21	E[2]	2120							1730	+375
		S	2545	1859	686	330	405	−41	375	2234	+311
52 (2001)	8.09	E[2]	2060							1640	+425
		S	2562	1834	728	290	390	−73	366	2200	+362
53 (2002)	8.48	E[3]	1960							1710	+255
		S	2614	1923	691	347	420	−11	362	2285	+329
54 (2003)	8.48	E[3]									+330
		S	2645	1919	735	279	376	−93	372	2291	+354

[1] From Humphreys et al. (2005) for September 1 to August 31. Accompanying simulated values are also for September 1 to August 31. The LAI measurements are of projected area.
[2] From Morgenstern et al. (2004).
[3] From Humphreys (2004).

The time course of N_2 fixation in the model was consistent with the observation by Jurgensen et al. (1992) that large amounts of woody residue in harvested stands accelerate non-symbiotic N_2 fixation to nearly double that in uncut stands. Plant N uptake during the model run remained limited by net N mineralization, including products of N_2 fixation, of about 1.5 g N m^{-2} $year^{-1}$ (apparent from declining SON in Figure 1a), plus total wet and dry deposition rates of about 0.25 g N m^{-2} $year^{-1}$. Therefore soil mineral N content and hence N leaching remained low until 120 years after clearcutting, after which N contents and leaching rose gradually (Figures 1a and 1b).

Plant water relations

The ability of Hypothesis 2 to explain forest age effects on energy and CO_2 exchange was examined during a warming period (July 21–24, 2002; DOY 202–205) when daytime T_a rose to 30 °C (Figure 2) and D rose from 1.5 to 3 kPa. Modeled and measured LE increased during warming in the 2000 stand (Figure 3a), apparent as a decline H/LE to about 1 during DOY 202–205 followed by a rise in H/LE during subsequent cooling (Figure 3d). Most energy exchange modeled in the 2000 stand was by deciduous bush, which transpired more rapidly with less sensitivity to D than did coniferous vegetation because of its smaller Ω_a and larger g_c. Changes in LE and H/LE with warming in the 1989 stand (Figures 3b and3e) were less apparent than those in the 2000 stand, although values of LE and H/LE were similar. The LE declined and H rose during warming in the 1949 stand, apparent in the lower LE modeled and measured during DOY 203–205 (Figure 3c). Rising H/LE modeled and measured under higher T_a and D with advancing forest age (Figures 3d–f) was attributed in the model partly to declining ψ_c and partly to the declining presence of deciduous vegetation.

Exchange of CO_2 was largely unaffected by warming in the 2000 and 1989 stands (Figures 4a and 4b), as was energy exchange (Figures 3a and 3b). In the 2000 stand, most CO_2 uptake modeled was by deciduous bush (Figure 1c). Influxes of CO_2 declined during warming in the 1949 stand, most notably during midafternoons, whereas CO_2 effluxes increased from rising R_h and R_a (Figure 4c). Daily aggregations of modeled and measured CO_2 fluxes in the 2000, 1989 and 1949 stands indicated that, during the warming event in July 2002, the

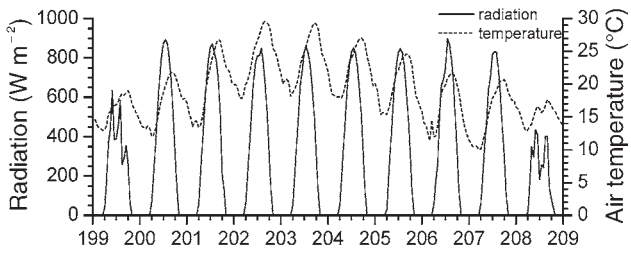

Figure 2. (a) Radiation and air temperature measured during DOY 200–209 (July 19–28) 2002 over Douglas-fir stands regenerating from clearcuts.

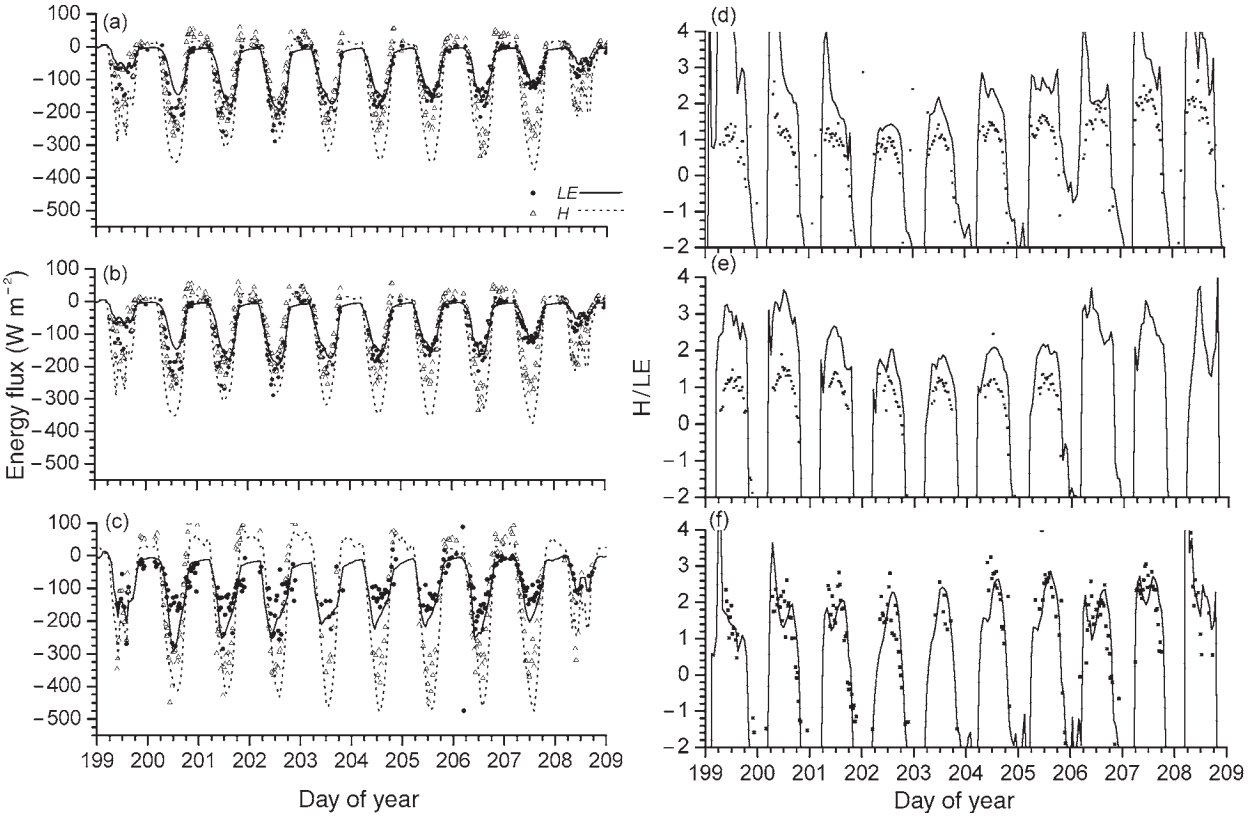

Figure 3. (a–c) Latent (LE) and sensible (*H*) heat fluxes, and (d–f) *H*/LE measured by eddy covariance (symbols) and modeled (lines) during DOY 200–209 (July 19–28) 2002 over Douglas-fir stands regenerating from clearcuts in (a, d) 2000, (b, e) 1989 and (c, f) 1949. Positive and negative values denote downward and upward fluxes respectively.

2000 stand remained a small source of CO_2, the 1989 stand changed from a small sink to a small source, and the 1949 stand changed from a large sink to a large source (Humphreys 2004; Figure 5). Such changes were also apparent during several other warming events in 2002. The adverse impact of warming on daily NEP of conifers has been observed in other studies (e.g., Grant et al. 2001*a*, Griffis et al. 2003, Morgenstern et al. 2004).

In the model, the effects of forest age on energy partitioning (Figure 3) and CO_2 exchange (Figure 4) were caused by age effects on plant water relations. These effects were examined during modeled stand development (14, 30, 53 and 109 years after clearcut, each of which ran under 2002 weather). Increasing bole height (z_b = 7, 19, 28 and 35 m, respectively) raised ψ_c as well as Ω_a, and so lowered bole hydraulic conductance (Figure 6a). Diurnal variation in Ω_a was caused by variation in root and stem radii associated with variation in ψ_r and ψ_c through bulk moduli of elasticity. Values of leaf specific bole hydraulic conductivity calculated from Ω_a , z_b and LAI (Figure 6b) were consistent with values derived experimentally in conifers (e.g. 10^{-3}–10^{-4} m^2 MPa^{-1} h^{-1} from Tyree and Ewers (1991) and Ewers and Zimmerman (1984)). Diurnal variation in stem axial conductivity was similar to that measured by Waring and Running (1978) in Douglas-fir during early summer. Higher ψ_c and Ω_a with z_b forced larger canopy–root water potential differences to sustain daytime water uptake, and delayed canopy recharge and recovery of ψ_c from overnight water uptake. These changes caused lower predawn and mid-afternoon ψ_c with increasing bole height (Figure 7a). Modeled midday ψ_c was similar to that measured in old-growth Douglas-fir of different heights by Bauerle et al. (1999). However modeled predawn ψ_c in older trees following days with large *D* was lower than that measured by Bauerle et al. (1999), because overnight recharge of tree water capacitance in the model was slowed by large conifer Ω_a. Incomplete recharge of bole water following periods of rapid transpiration was found by Waring and Running (1978) to lower bole water content of Douglas-fir during the summer, which may have resulted in the declines in predawn ψ_c of Douglas-fir measured by Waring and Running (1978) as summer progressed. Predawn ψ_c in the model gradually returned to higher values during the week following a period of high *D* (e.g., during DOY 206–209 following high T_a during DOY 202–205 in Figure 7a). Lower ψ_c with advancing age forced greater declines in g_c (Figure 7b) and hence CO_2 uptake (Figure 7c) at high *D*, especially during midafternoons. Midday declines in g_c, even more pronounced than those modeled here, were measured in taller (50–60 m) Douglas-fir stands by Waring and Running (1978).

Lower ψ_c modeled in older forests forced greater shoot–root transfers of nonstructural C $\sigma_{Ci,j}$ that raised NPP_{root}:NPP_{shoot} from 0.22 through 0.25 to 0.43 for the 30-, 53- and 109-year-old stands, respectively. This rise was consistent with the

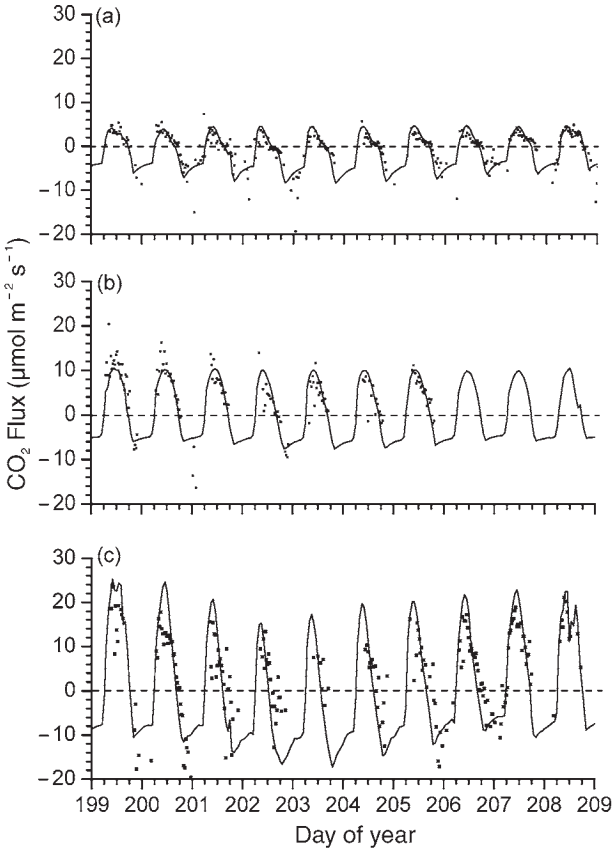

Figure 4. Fluxes of CO_2 measured by eddy covariance (symbols) and modeled (lines) during DOY 200–209 (July 19–28) 2002 over Douglas-fir stands regenerating from clearcuts in (a) 2000, (b) 1989 and (c) 1949. Positive and negative values denote downward and upward fluxes, respectively.

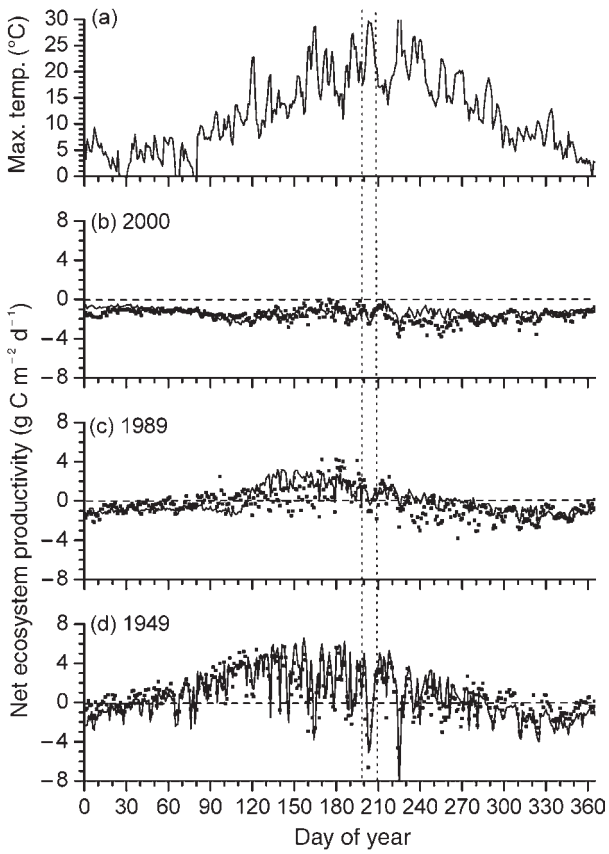

Figure 5. (a) Maximum daily air temperature, and daily net ecosystem productivity (NEP) from gap-filled eddy covariance measurements (symbols) and modeled (lines) during 2002 over Douglas-fir stands regenerating from clearcuts in (a) 2000, (b) 1989 and (c) 1949. Vertical lines indicate warming period.

experimental findings of Ryan et al. (2004) that below-ground C allocation increases with stand age.

Primary productivity and autotrophic respiration

The R_a:GPP ratio increased during the first 60 years of forest growth, remained stable for the next 60 years, and then declined (Figure 8). During forest aging, lower ψ_c (Figure 7a) forced lower g_c (Figure 7b) and hence lower GPP (Figure 7c), especially at high D (DOY 202–205 in Figure 7c). Lower GPP caused lower plant nonstructural C content, σ_C, and hence lower respiration of σ_C (R_c). Meanwhile uptake and accumulation of N in phytomass during early forest growth raised maintenance respiration (R_m), which with lower R_c eventually forced lower growth respiration R_g and accelerated respiration of remobilized foliar C, R_s, thereby accelerating litterfall. Rising litterfall lowered LAI (Figure 1d), foliar C, and hence foliar N, which prevented further rises in R_m, R_s and R_a. Wood N continued to rise, but because only N in an outer layer of the bole and branches was maintained, the gain in wood N did not offset the loss of foliar and twig N from accelerated litterfall in determining R_m. Therefore declines in R_m and hence R_a were commensurate with those in GPP caused by hydraulic limitations (Figure 1c), so that R_a:GPP remained stable more than 60 years after clearcutting (Figure 8). Thus the model adjusted foliar mass so that foliar respiration was in balance with its primary productivity. Declines in NPP modeled during later growth were attributed mostly to declining GPP (Figure 1c) rather than rising R_a:GPP, as found experimentally by Ryan et al. (2004).

Greater litterfall modeled during forest aging caused more rapid decomposition D_S and release of DOC, maintaining R_h, R_g and microbial growth, even while GPP declined. Consequently CO_2 effluxes (= R_a + R_h) rose more than CO_2 influxes during forest aging (Figure 7c).

Forest age and net ecosystem productivity

All three hypotheses contributed to the time course of NEP modeled after clearcutting. During the first 4 years after clearcutting, rapid R_h from fine and coarse litter raised ecosystem respiration R_e (= R_a + R_h) while GPP remained low, so that estimated and modeled NEP (= GPP–R_e) indicated net C losses of 500 to 750 g C m^{-2} $year^{-1}$ (Table 2; Figure 9a). During this pe-

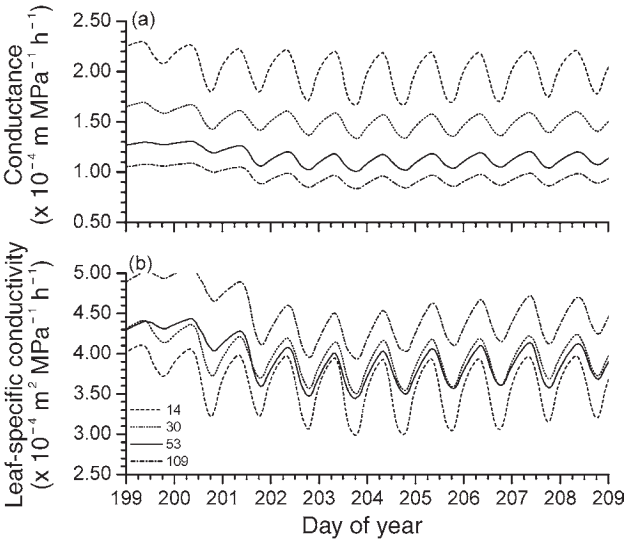

Figure 6. (a) Hydraulic conductance and (b) leaf specific conductivity of Douglas-fir stems modeled during DOY 200–209 (July 19–28) 2002 over Douglas-fir stands 14, 30, 53 and 109 years after clearcutting.

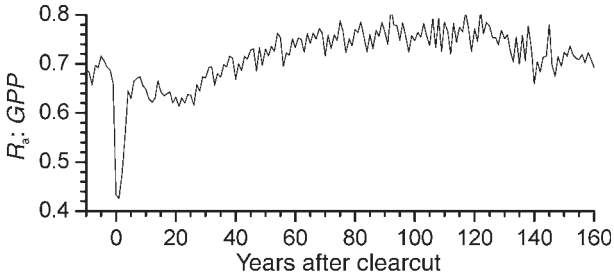

Figure 8. Ratio of autotrophic respiration to GPP (R_a:GPP) modeled during 160 years of Douglas-fir regrowth following clearcutting.

riod, the model indicated that the rapid losses of soil C, mostly from litter, were not offset by gains in wood C (Figure 9b).

Annual GPP and R_e rose slowly during the next decade while N was being immobilized in the woody litter (Table 2; Figure 1a). During this period, R_h and soil C losses slowed so that NEP rose rapidly (Figure 9a) even though gains in wood C were small (Figure 9b). The forest stand was estimated and modeled to be a small source of C after 13 years (Table 2), and remained nearly C neutral until the onset of net N mineraliza-

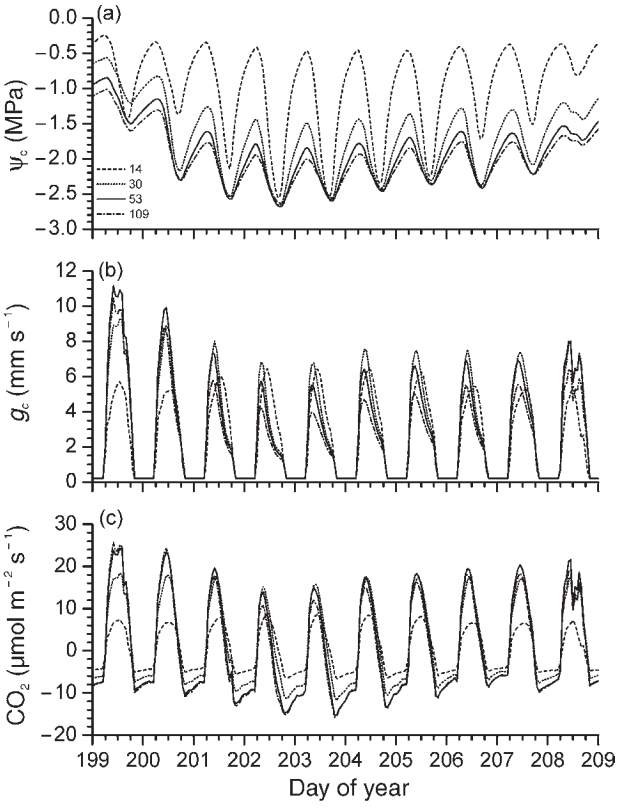

Figure 7. (a) Canopy water potential ψ_c, (b) canopy stomatal conductance g_c and (c) CO_2 flux modeled during DOY 200–209 (July 19–28) 2002 over Douglas-fir stands 14, 30, 53 and 109 years after clearcutting. Positive and negative values denote downward and upward fluxes, respectively.

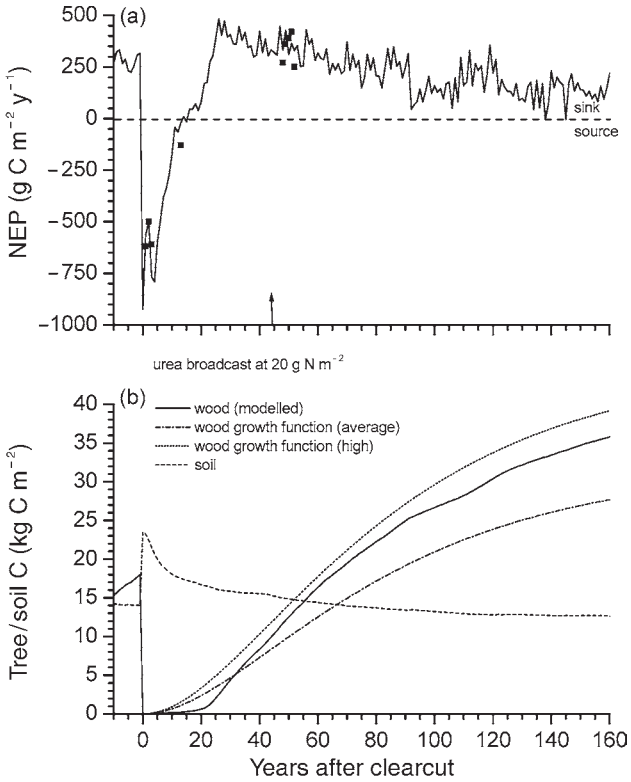

Figure 9. (a) Net ecosystem productivity (NEP) modeled during 160 years of Douglas-fir regrowth following clearcutting (line), and estimated from gap-filled eddy covariance measurements of CO_2 flux in a post-clearcut Douglas-fir chronosequence (symbols). (b) Aboveground C and soil C modeled by *ecosys* and calculated from a growth function fitted to measurements of aboveground forest C by Janisch and Harmon (2002) during 160 years of Douglas-fir regrowth following clearcutting.

tion after 20 years (Figure 1a) caused NEP to rise rapidly (Figure 9a). Thereafter declines in soil C slowed while gains in wood C rose (Figure 9b). Values of GPP and R_e estimated from EC data remained less than modeled values, but differences between GPP and R_e were similar so that both estimated and modeled NEP reached 200–400 g C m^{-2} $year^{-1}$ by 50 years after clearcutting (Table 2; Figure 9a). Both estimated and modeled R_e rose more than GPP in warmer years (e.g., at 49 years in 1998 when MAT was 9.1 °C) than in cooler years (e.g., at 50 years in 1999 when MAT was 7.6 °C) so that warming caused annual NEP to decline (Table 2). This decline in NEP of mature forests with warming was also apparent in hourly (Figure 4c) and daily (Figure 5d) C fluxes, and was attributed to hydraulic effects on ψ_c, g_c and hence GPP (Figure 7c), as well as to temperature effects on R_m and R_h. Modeled NEP declined in older stands, reaching about 1/2 of their maximum values after 120 years (Figure 9a). During this period, wood C gain declined, partly because of reduced GPP and partly because of greater NPP_{root}:NPP_{shoot} caused by declining ψ_c (Figure 7a). During the entire post-harvest growth cycle, modeled wood C remained between values from wood C growth curves derived by Janisch and Harmon (2002) from allometric measurements of Douglas-fir stands with differing productivity in nearby Washington state (Figure 8b).

Values of annual GPP and R_e in the model usually exceeded those estimated from EC data (Table 2). The estimated values depended on assumptions used in gap-filling, and may have been reduced by incomplete energy balance closure; consequently these values may underestimate actual fluxes.

Effect of vegetation and residue management on forest NEP

Removal of pioneer bush hastened the recovery of NEP (Figure 10a) and growth of wood (Figure 10b) in the modeled Douglas-fir stand over that without bush removal, although long-term NEP and growth were similar. In the model, bush removal reduced competition for mineral N during immobilization after clearcutting (Figure 1b). Removal of most foliar and non-woody residue during clearcutting delayed the recovery of NEP (Figure 10a) and growth of wood (Figure 10b) over that with little residue removal, although long-term growth was little affected. In the model, increased removal of residue reduced N mineralization during the first three years after clearcutting (Figure 1a), and thereby slowed Douglas-fir growth. These model results were consistent with the experimental findings of Roberts et al. (2005) concerning the effects of harvest residue and competing vegetation on Douglas-fir seedling growth.

Effect of logging frequency on forest NEP

The NEP in the 120-year logging cycle was larger than that in the 60-year cycle for about 20 years after the forest in the 60-year cycle was logged, but was smaller during the remainder of the cycle because NEP declined with forest age (Figure 11a). These differences in NEP largely offset each other so that lengthening the harvest cycle from 60 to 120 years reduced wood C removal (Figure 11b) and raised soil C retention (Figure 11c) by only about 30 g m^{-2} $year^{-1}$ (Table 3). More coarse woody residue left after logging in the 120-year cycle (Figure 11c) lengthened the period of N immobilization,

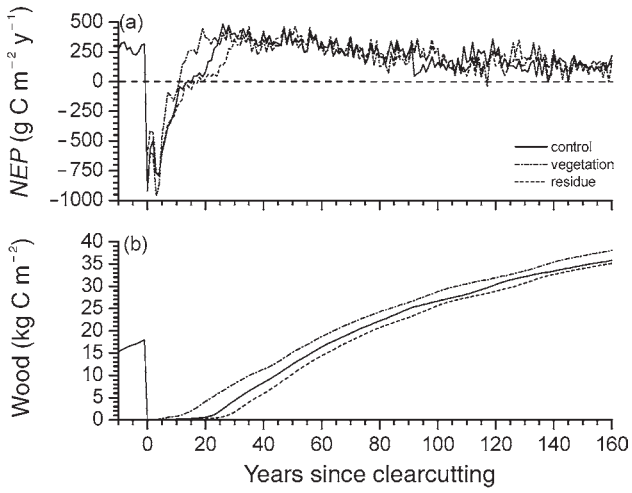

Figure 10. (a) Net ecosystem productivity (NEP) and (b) wood growth modeled during 160 years of Douglas-fir regrowth following clearcutting as affected by removal of competing pioneer vegetation or of aboveground non-woody residue.

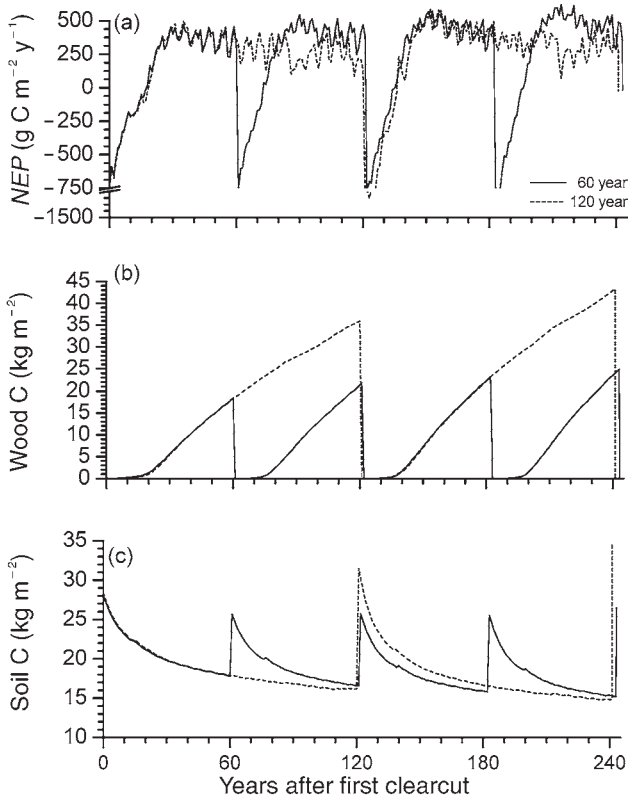

Figure 11. (a) Net ecosystem productivity (NEP), (b) wood C and (c) soil C of a Douglas-fir stand modeled during four clearcutting cycles of 60 years or two clearcutting cycles of 120 years.

and so raised C losses and delayed NEP recovery (Figure 11a). Less removal of wood C and greater retention of residue C in the 120-year cycle caused gains in soil C to be modeled after two 120-year cycles rather than losses after four 60-year cycles (Table 3; Figure 11c). Wood C removal and residue C return in the model increased slightly with each successive harvest in the 60-year and the 120-year logging cycles (Figures 11b and11c) because N removals in wood and slash were slightly smaller than N inputs from wet and dry atmospheric deposition plus biological fixation (Figure 1b). This model result is consistent with observations of gradual N enrichment at harvested sites in which most slash is left on the ground (Likens and Bormann 1995).

Discussion

Plant litter decomposition and plant N uptake

The early rise and subsequent decline in soil N availability in the model (Figure 1) is characteristic of the assart effect frequently observed in clearcut sites (Kimmins 2004). Bradley et al. (2002) found larger mineral N concentrations in the soils of 5 year post-clearcut sites than in those of 8, 12, and 28 year sites in the nearby Pacific silver fir and western hemlock forest zone of Vancouver Island, indicating early net N mineralization followed by N immobilization. Bradley et al. (2002) corroborated this finding by measuring declines in Pacific fir needle N concentrations from 1.2% at 4-year post-clearcut sites to 0.9 and 0.8% at 7- and 11-year sites. Douglas-fir needle N concentrations modeled in this study declined from 1.4% 4 years after clearcutting to 1.1 and 0.9% 7 and 11 years after clearcutting (assuming needle DM is 43% C), in response to declining soil N availability (Figure 1a). These needle N concentrations were constrained in the model by competition for soil N uptake with deciduous pioneer vegetation (Figure 10), as found experimentally by Roberts et al. (2005). During later mineralization from the woody litter complex in the model, needle N concentrations increased gradually from 0.9 to 1.4% between 11 and 60 years after clearcutting, indicating the gradual alleviation of earlier N constraints. Similarly, Kimmins et al. (2002) found that the most rapid rise in growth and N accumulation by Pacific fir–western hemlock stands on Vancouver Island occurred between 10 and 26 years after clearcutting. These findings tend to corroborate Hypothesis 1 as represented in Figure 1. The rates at which both fine and coarse litter decompose and mineralize after clearcutting must therefore be accurately modeled if stand regeneration after clearcutting is to be accurately modeled (Figures 8 and 9a; Table 2). However these rates do not explain later declines in NPP.

Table 3. Changes in carbon stocks (g C m^{-2}) of a Douglas-fir forest stand modeled after four logging cycles of 60 years each or two logging cycles of 120 years each. Abbreviations: DOC = dissolved organic carbon; DIC = dissolved inorganic carbon; and NEP = net ecosystem production.

Δ C Stock	4 × 60 Years	2 × 120 Years
Removal of wood	53425	45592
Removal of other material	432	160
Δ Soil	–2400	+5398
DOC Export	447	447
DIC Export	1252	1366
Total NEP	53156	52963

Plant water relations

Gradual declines in GPP (Figure 1c) and hence NEP (Figure 9a) modeled more than 60 years after clearcutting were attributed in the model to lower ψ_c forced by rising Ω_a with increasing tree height (Figure 6a). Such changes have frequently been reported in other coniferous forest stands. McDowell et al. (2002) measured declines of 44% in hydraulic conductivity and 0.5 MPa in ψ_c of Douglas-fir as tree height increased from 15 to 60 m among differently aged Douglas-fir–western hemlock stands in nearby Washington, USA, although they did not find that g_c and CO_2 uptake measured by portable cuvette were more sensitive to *D*. However Chen et al. (2002) found greater reductions in CO_2 uptake at high *D* when analyzing EC fluxes measured over older versus younger stands also in Washington, USA. Hubbard et al. (1999) found that mean hydraulic conductivity of ponderosa pine declined by 63% as height increased from 10 to 30 m (cf. Figure 6a), causing g_c (cf. Figure 7b) and GPP (cf. Figure 4c versus 4b) to decline more rapidly in response to rising *D* in older trees than in younger trees. Lower g_c and GPP modeled in taller trees are consistent with greater stomatal constraints to GPP inferred from lower $\delta^{13}C$ depletion measured in taller trees by Fessenden and Ehleringer (2002), Hubbard et al. (1999), McDowell et al. (2002), and others. These findings tend to corroborate model Hypothesis 2 as represented in Figures 3–7. However, Hypothesis 2 allows g_c and CO_2 uptake to be larger in older, taller forests at moderate *D* if their photosynthetic capacity is greater than that of younger shorter forests as proposed by Ryan and Yoder (1997).

Larger sapwood area has been proposed to offset partially or fully the effect of greater bole length on tree hydraulic conductance during growth (e.g., Becker et al. 2000) as found in Douglas-fir by Phillips et al. (2002), and McDowell et al. (2002). The model accounts to some extent for the offsetting effect of sapwood area on conductance during growth by linking Ω_a to maximum foliar area (Figure 6b), and by increasing bole water capacitance with bole mass (Figure 7a). However, modeled LAI reached its maximum value (about 8) between 20 and 40 years after clearcutting and declined gradually thereafter (Figure 1d), so that the LAI effect on Ω_a was absent during later growth. Increases in sapwood conductivity not associated with increases in foliar area are not simulated in *ecosys*, and so the model may overestimate height effects on tree water status. Nonetheless, accurately modeling of height effects on g_c through their effects on ψ_c–ψ_σ gradients and bole W_a, as required in Hypothesis 2, appears necessary for modeling age effects on forest growth.

Gross primary productivity and autotrophic respiration

The model stabilized ratios of R_a:GPP (Figure 8) by accelerating foliar C and N litterfall, and so reducing foliar C, N and LAI (Figure 1d), and hence R_a. Declines in GPP and LAI as modeled here are frequently found in aging forests (Ryan et al. 1997, Smith and Resh 1999). The stable ratio of R_a:GPP in the model, even while GPP was declining, indicate that rising R_a did not drive the decline in modeled wood growth with age (Figure 9b), as has also been found experimentally by Ryan et al. (2004). This stable ratio in the model is consistent with the general observation of Waring and Running (1998) that R_a:GPP is conserved in forests of differing ages in a variety of temperate climates. The ratio modeled here (0.70–0.75, depending on yearly weather) was larger than that simulated in other forests (e.g., Grant et al. 1999*a*, 2001*a*) because of the large needle mass and hence needle N maintained in the modeled Douglas-fir stand. The model did not require a continuous rise in R_a:GPP as proposed in Hypothesis 3 to model declining GPP and NEP with advancing forest age.

Changes in forest NPP caused changes in modeled bole mass with age that could be tested against bole volume growth curves for coastal Douglas-fir stands with a site index of 35 (that of the sites in this study) derived from inventory measurements with the Table Interpolation Program for Stand Yields (TIPSY) v. 3.0 (Mitchell et al. 2000). For a mean wood density of 0.45 Mg m^{-3} (Gartner et al. 2002) and a C content of 0.5, these volume growth curves indicate that bole mass growth of coastal Douglas-fir reaches peak rates of 450 g C m^{-2} $year^{-1}$ between 40 and 60 years of age, and then declines to 225 g C m^{-2} $year^{-1}$ at 150 years of age. Wood growth in the model reached maximum rates of 400–440 g C m^{-2} $year^{-1}$ between 45 and 55 years after logging (Table 2), but declined to 200 g C m^{-2} $year^{-1}$ between 140 and 150 years after logging (Figure 9b). Wood C growth in the model remained within the range of growth curves derived by Janisch and Harmon (2002) from allometric measurements of wood C in Douglas-fir-western hemlock forests in nearby Washington State (Figure 9b). Aboveground C in the model 53 years after the second clearcut was 14.4 kg m^{-2}, consistent with measurements of about 15 kg m^{-2} at the 1949 site in 2002. These comparisons indicate that modeled wood growth, a key component of forest NEP, was consistent with long-term inventory measurements.

Effect of land use practices on forest NEP

The time course of NEP modeled in Figures 10 and 11 was based on some key assumptions. (1) *Ecosys* does not yet simulate gap replacement, so that once the pioneer deciduous population in the model was suppressed by the Douglas-fir population about 20 years after clearcutting (Figure 1c), the model proceeded to simulate an even-aged Douglas-fir stand with no understory. Such a stand may be appropriate for replanted Douglas-fir in this study, which maintains a sparse understory when more than 20 years old. However, naturally regenerated stands are more complex, especially at more advanced ages when the simulation of simple stands might introduce a bias toward lower NEP. (2) *Ecosys* allows seeding and thinning operations to be applied during model runs to user-selected species on user-selected dates in complex biomes. These operations were used in this study to simulate mortality by prescribing annual reductions of overstory and understory populations during model runs. However the time course of natural mortality may be influenced by site characteristics or climate events not amenable to prescription. (3) The fractions of non-woody and woody material removed during logging was the same in both 60-year and 120-year cycles (0.1 and 0.6 respectively). These fractions were consistent with measurements of wood C removed versus woody litter C left on site after clearcutting Douglas-fir (e.g., Janisch and Harmon 2002). If these fractions had been larger in the 120-year cycle than in the 60-year cycle, then wood C removals in the 120-year cycle would have been larger, and soil C gains smaller, than those in Table 3. Site measurements from which to derive these fractions are currently scarce, and more measurements of how much non-woody and woody C is removed versus left on site under different harvest practices need to be made for future projections of harvest effects on NEP.

Four main conclusions can be drawn from our study. (1) Nutrient uptake in *ecosys* changed during forest regeneration because of different time scales for decomposition of fine, non-woody and coarse woody litter left after harvesting. The model attributed an initial rise in GPP observed during the first 3 years after clearcutting to nutrient mineralization from rapid decomposition of fine, non-woody litter that exceeded nutrient immobilization during early decomposition of coarse woody litter with higher C:N ratios. The model attributed a slower rise in GPP during the next 20 years to immobilization during later decomposition of coarse woody litter that exceeded mineralization from decomposition of fine, non-woody litter. The model attributed a rapid rise in GPP between 20 and 40 years after clearcutting to nutrient mineralization with further decomposition of coarse woody litter and of its decomposition products. (2) Axial hydraulic conductance in *ecosys* declined with lengthening of the water uptake pathway during bole and branch growth. This decline forced lower canopy water potentials and hence greater sensitivity of stomatal conductances and CO_2 uptake to D, as also found in EC measurements. (3) The R_a:GPP ratio in *ecosys* did not rise with phytomass accumulation, and so changes in this ratio did not explain forest age effects on NEP. (4) Removal of pioneer vegetation and non-woody residue, respectively, hastened and delayed rises in NEP and wood growth after clearcutting, although long-term effects of removal on wood mass was not large. Changes in NEP modeled with forest age caused less wood C to be removed, and more soil C to be retained, during 120-year clearcutting cycles than during 60-year clearcutting cycles.

References

Amiro, B.D. 2001. Paired-tower measurements of carbon and energy fluxes following disturbance in the boreal forest. Global Change Biol. 7:253–268.

Amiro, B.D., J.I. MacPherson and R.L. Desjardins. 1999. BOREAS flight measurements of forest-fire effects on carbon dioxide and energy fluxes. Agric. For. Meteorol. 96:199–208.

Barnes, B.V., D.R. Zak, S.R. Denton and S.H. Spurr. 1998. Forest Ecology 4th edn. Wiley and Sons. New York, 447 p.

Bauerle, W.L., T.M. Hinckley, J. Čermák, J. Kučera and K. Bible. 1999. The canopy water relations of old growth Douglas-fir trees. Trees 13:211–217.

Becker, P., F.C. Meinzer and S.C. Wullschleger. 2000. Hydraulic limitation of tree height: a critique. Funct. Ecol. 14:4–11.

Bradley, R.L., J.P. Kimmins and W.L. Martin. 2002. Post-clearcutting chronosequence in the B.C. Coastal Western Hemlock Zone. II. Tracking the assart flush. J. Sust. For. 14:23–43.

Brock, T.D. and M.T. Madigan. 1991. Biology of microorganisms 6th. Edn. Prentice Hall, NJ, 874 p.

Cannell, M.G.R. 1989. Physiological basis of wood production: a review. Scand. J. For. Res. 4:459–490.

Chen, H., M.E. Harmon and R.P. Griffiths. 2001. Decomposition and nitrogen release from decomposing woody roots in coniferous forests of the Pacific Northwest: A chronosequence approach. Can. J. For. Res. 31:246–260.

Chen, J., M. Falk, E. Euskirchen, K.T. Paw U, T.H. Suchanek, S.L. Ustin, B.J. Bond, K.D. Brosofske, N. Phillips and R. Bi. 2002. Biophysical controls of carbon flows in three sucessional Douglas-fir stands based on eddy covariance measurements. Tree Physiol. 22:169–177.

Cohen, W.B., M.E. Harmon, D.O. Wallin and M. Fiorella. 1996. Two decades of carbon fluxes from forests of the Pacific northwest. Bioscience 46:836–844.

Doussan, C., G. Vercambre and L. Pagès. 1998. Modeling of the hydraulic architecture of root systems: An integrated approach to water absorption—distribution of axial and radial conductances in maize. Ann. Bot. 81:225–232.

Ewers, F.W. and M.H. Zimmermann. 1984. The hydraulic architecture of eatern Hemlock (*Tsuga canadiensis*). Can. J. Bot. 62: 940–946.

Farquhar, GD, S. von Caemmerer and J.A. Berry. 1980. A biochemical model of photosynthetic CO_2 assimilation in leaves of C_3 species. Planta 149:78–90.

Fessenden, J.E. and J.R. Ehleringer. 2002. Age-related variations in $\delta^{13}C$ of ecosystem respiration across a coniferous forest chronosequence in the Pacific Northwest. Tree Physiol. 22:159–167.

Gartner, B.L., E.M. North, G.R. Johnson and R. Singleton. 2002. Effects of live crown on vertical patterns of wood density and growth in Douglas-fir. Can. J. For. Res. 32:439–447.

Grant, R.F. 1989. Test of a simple biochemical model for photosynthesis of maize and soybean leaves. Agric. For. Meteorol. 48: 59–74.

Grant, R.F. 1991. The distribution of water and nitrogen in the soil-crop system: A simulation study with validation from a winter wheat field trial. Fert. Res. 27:199–214.

Grant, R.F. 1994. Simulation of ecological controls on nitrification. Soil Biol. Biochem. 26:305–315.

Grant, R.F. 1995*a*. Mathematical modeling of nitrous oxide evolution during nitrification. Soil Biol. Biochem. 27:1117–1125.

Grant, R.F. 1995*b.* Salinity, water use and yield of maize: Testing of the mathematical model *ecosys*. Plant Soil. 172:309–322.

Grant, R.F. 1998*a*. Simulation of methanogenesis in the mathematical model *ecosys.* Soil Biol. Biochem. 30:883–896.

Grant, R.F. 1998*b.* Simulation in *ecosys* of root growth response to contrasting soil water and nitrogen. Ecol. Model. 107:237–264.

Grant, R.F. 1999. Simulation of methanotrophy in the mathematical model *ecosys.* Soil Biol. Biochem. 31:287–297.

Grant, R.F. 2001. A review of the Canadian ecosystem model *ecosys*. *In* Ed. M. Shaffer. Modeling carbon and nitrogen dynamics for soil management. CRC Press, Boca Raton, FL, pp 175–264.

Grant, R.F. and P. Rochette. 1994. Soil microbial respiration at different temperatures and water potentials: Theory and mathematical modeling. Soil Sci. Soc. Am. J. 58:1681–1690.

Grant, R.F. and J.A. Robertson. 1997. Phosphorus uptake by root systems: mathematical modeling in *ecosys.* Plant Soil 188: 279–297.

Grant, R.F. and E. Pattey. 1999. Mathematical modeling of nitrous oxide emissions from an agricultural field during spring thaw. Global Biogeochem. Cycles 13:679–694.

Grant, R.F. and N.T. Roulet. 2002. Methane efflux form boreal wetlands: Theory and testing of the ecosystem model *ecosys* with chamber and tower flux measurements. Global Biogeochem. Cycles 16:1054.

Grant, R.F. and E. Pattey. 2003. Modeling variability in N_2O emissions from fertilized agricultural fields. Soil Biol. Biochem. 35:225–243.

Grant, R.F., N.G. Juma and W.B. McGill. 1993*a*. Simulation of carbon and nitrogen transformations in soils. I. Mineralization. Soil Biol. Biochem. 27:1317–1329.

Grant, R.F., N.G. Juma and W.B. McGill. 1993*b.* Simulation of carbon and nitrogen transformations in soils. II. Microbial biomass and metabolic products. Soil Biol. Biochem. 27:1331–1338.

Grant, R.F., R.L. Garcia, P.J. Pinter, D. Hunsaker, G.W. Wall, B.A. Kimball and R.L. LaMorte. 1995*a*. Interaction between atmospheric CO_2 concentration and water deficit on gas exchange and crop growth: Testing of *ecosys* with data from the Free Air CO_2 Enrichment (FACE) experiment. Global Change Biol. 1:443–454.

Grant, R.F., B.A. Kimball, P.J. Pinter, Jr., G.W. Wall, R.L. Garcia, R.L. LaMorte and D.J. Hunsaker. 1995*b.* CO_2 effects on crop energy balance: testing *ecosys* with a free air CO_2 enrichment (FACE) experiment. Agron. J. 87:446–457.

Grant, R.F., T.A. Black, G. den Hartog, J.A. Berry, S.T. Gower, H.H. Neumann, P.D. Blanken, P.C. Yang and C. Russell. 1999*a*. Diurnal and annual exchanges of mass and energy between an aspen-hazelnut forest and the atmosphere: testing the mathematical model *ecosys* with data from the BOREAS experiment. J. Geophys. Res. 104:27,699–27,717.

Grant, R.F., G.W. Wall, B.A. Kimball, K.F.A. Frumau, P.J. Pinter, Jr., D.J. Hunsaker and R.L. Lamorte. 1999*b.* Crop water relations under different CO_2 and irrigation: testing of *ecosys* with the free air CO_2 enrichment (FACE) experiment. Agric. For. Meteorol. 95:27–51.

Grant, R.F., M.L. Goulden, S.C. Wofsy and J.A. Berry. 2001*a*. Carbon and energy exchange by a black spruce–moss ecosystem under changing climate: testing the mathematical model *ecosys* with data from the BOREAS experiment. J. Geophys. Res. 106:33,605-33,621.

Grant, R.F., B.A. Kimball, T.J. Brooks et al. 2001*b.* CO_2 effects on mass and energy exchange of wheat under different N fertilization: model theory and testing with a Free Air CO_2 Enrichment (FACE) experiment. Agron. J. 93:638–649.

Grant, R.F., W.C. Oechel, C. Ping and H. Kwon. 2003. Carbon balance of coastal arctic tundra under changing climate. Global Change Biol. 9:16–36.

Grant, R.F., B.A. Kimball, G.W. Wall et al. 2004. How elevated CO_2 affects water relations, water use and growth of irrigated sorghum: testing a model with results from a Free Air CO_2 Enrichment (FACE) experiment Agron. J. 96: 1693–1705.

Griffis, T.J., T.A. Black, K. Morgenstern, A.G. Barr, Z. Nesic, G.B. Drewitt, D. Gaumont-Guay and J.H. McCaughey. 2003. Ecophysiological controls on the carbon balances of three southern boreal forests. Agric. For. Meteorol. 117:53–71.

Hubbard, R.M., B.J. Bond and M.G. Ryan. 1999. Evidence that hydraulic conductance limits photosynthesis in old *Pinus ponderosa* trees. Tree Physiol. 19:165–172.

Humphreys, E.R. 2004. Net ecosystem production of three coastal Douglas-fir stands at different stages of development after harvesting. Ph.D. Thesis. University of British Columbia, 122 p.

Humphreys, E.R., T.A. Black, G.J. Ethier, G.B. Drewitt, D.L. Spittlehouse, E.-M. Jork, Z. Nesic and N.J. Livingston. 2003. Annual and seasonal variability of sensible and latent heat fluxes above a coastal Douglas-fir forest, British Columbia, Canada. Agric. For. Meteorol. 115:109–125.

Humphreys, E.R., T.A. Black, K. Morgenstern, Z. Li and Z. Nesic. 2005. Net ecosystem production of a Douglas-fir stand for three years following clearcut harvesting. Global Change Biol. 11: 450–464.

Janisch, J.E. and M.E. Harmon. 2002. Successional changes in live and dead wood carbon stores: implications for net ecosystem productivity. Tree Physiol. 22:77–89.

Jurgensen, M.F., R.T. Graham, M.J. Larsen and A.E. Harvey. 1992. Clear-cutting, woody residue removal, and nonsymbiotic nitrogen fixation in forest soils of the Inland Pacific Northwest. Can. J. For. Res. 22:1172–1178.

Kelliher, F.M., C. Wirth, C. Rebmann et al. 1999. Productivity of forests in the Eurosiberian boreal region and their potential to act as a carbon sink—a synthesis. Global Change Biol. 5:703–722.

Kimmins, J.P. 2004. Forest ecology: a foundation for sustainable forest management and environmental ethics in forestry. 3rd Edn. Pearson Prentice Hall, NJ, 611 p.

Kimmins, J.P., W.L. Martin and R.L. Bradley. 2002. Post-clearcutting chronosequence in the B.C. Coastal Western Hemlock Zone. III. Sinks for mineralised or dissolved organic N. J. Sust. For. 14: 45–68.

Kowalski, S., M. Sartore, R. Burlett, P. Berbigier and D. Loustau. 2003. The annual carbon budget of a French pine forest (*Pinus pinaster*) following harvest. Global Change Biol. 9:1051–1065.

Kurz, W.A. and M.J. Apps. 1994. The carbon budget of Canadian forests: a sensitivity analysis of changes in disturbance regimes, growth rates and decomposition rates. Environ. Pollut. 83:55–61.

Kurz, W.A. and M.J. Apps. 1999. A 70 year retrospective analysis of carbon fluxes in the Canadian forest sector. Ecol. Appl. 9: 526–547.

Larcher, W. 2001. Physiological Plant Ecology. 4th Edn. Springer-Verlag, Berlin, 513 p.

Li, Z., M.J. Apps, E. Banfield and W.A. Kurz. 2002. Estimating net primary production in the Canadian prairie provinces using an inventory-based carbon budget model. Can. J. For. Res. 32:161–169.

Likens, G.E. and F.H. Bormann. 1995. Biogeochemistry of a forest ecosystem. 2nd Edn. Springer-Verlag, New York, 159 p.

Litvak, M., S. Miller, S.C. Wofsy and M. Goulden. 2003. Effect of stand age on whole system CO_2 exchange in the Canadian boreal forest. J. Geophys. Res. 108, NO. D3, 8225, doi: 10,1029/2001JDD000854.

Mäkelä, A. and H.T. Valentine. 2001. The ratio of NPP to GPP: evidence of change over the course of stand development. Tree Physiol. 21:1015–1030.

McDowell, N.G., N. Phillips, C. Lunch, B.J. Bond and M.G. Ryan. 2002. An investigation of hydraulic limitation and compensation in large, old Douglas-fir trees. Tree Physiol. 22:763–774.

Mitchell, K.J., M. Stone, S.E. Grout et al. 2000. TIPSY version 3.0. British Columbia Ministry of Forests Research Branch, Victoria, BC.

Morgenstern, K., T.A. Black, E.R. Humphreys, T.J. Griffis, G.B. Drewitt, T. Cai, Z. Nesic, D.L. Spittlehouse and N.J. Livingston. 2004. Sensitivity and uncertainty in the carbon balance of a Pacific northwest Douglas-fir forest during an El Niño/El Niña cycle. Agric. For. Meteorol. 123:210–219.

Peng, C., J. Liu, Q. Dang, M.J. Apps and H. Jiang. 2002. TRIPLEX: a generic hybrid model for predicting forest growth and carbon and nitrogen dynamics. Ecol. Model. 153:109–130.

Perämäki, M., E. Nikinmaa, S. Sevanto, H. Ilvesniemi, E. Siivola, P. Hari and T. Vesala. 2001. Tree stem diameter variations and transpiration in Scots pine: an analysis using a dynamic sap flow model. Tree Physiol. 21:889–897.

Phillips, N., B.J. Bond, N.G. McDowell and M.G. Ryan. 2002. Canopy hydraulic conductance in young, mature and old Douglas-fir trees. Tree Physiol. 22:205–211.

Pruyn, M.L., B.L. Gartner and M.E. Harmon. 2000. Respiratory potential of sapwood in old vs. young coniferous trees. *In* Abstracts of the Ecol. Soc. Am. 85th Ann. Gen. Meet., Washington, DC 180 p.

Pypker, T.G. and A.L. Fredeen. 2002*a*. Ecosystem CO_2 flux over two growing seasons for a sub-Boreal clearcut 5 and 6 years after harvest. Agric. For. Meteorol. 114:15–30.

Pypker, T.G. and A.L. Fredeen. 2002*b*. The growing season carbon balance of a sub-boreal clearcut 5 years after harvesting using two independent approaches to measure ecosystem CO_2 flux. Can. J. For. Res. 32:852–862.

Rannik, U., N. Altimir, J. Raittila et al. 2002. Fluxes of carbon dioxide and water vapour over Scots pine forest and clearing. Agric. For. Meteorol. 111:187–202.

Roberts, S.D., C.A. Harrington and T.A. Terry. 2005. Harvest residue and competing vegetation affect soil moisture, soil temperature, N availability, and Douglas-fir seedling growth. For. Ecol. Manage. 205:333–350.

Ryan, M.G. and R.H. Waring. 1992. Maintenance respiration and stand development in a subalpine lodgepole pine forest. Ecol. 73:2100–2108.

Ryan, M.G. and B.J. Yoder. 1997. Hydraulic limits to tree height and tree growth. Bioscience 47:235–242.

Ryan, M.G., D. Binkley and J.H. Fownes. 1997. Age-related decline in forest productivity: pattern and process. Adv. Ecol. Res. 27: 213–262.

Ryan, M.G., D. Binkley, J.H. Fownes, C.P. Giardina and R.S. Senock. 2004. An experimental test of the causes of forest growth decline with stand age. Ecol. Monogr. 74:393–414.

Schimel, J.P. and M.K. Firestone. 1989. Nitrogen incorporation and flow through a coniferous forest soil profile. Soil Sci. Soc. Am. J. 533:779–784.

Schulze, E.-D., J. LLoyd, F.M. Kelliher et al. 1999. Productivity of forests in the Eurosiberian boreal region and their potential to act as a carbon sink—A synthesis. Global Change Biol. 5:703–722.

Shulten, H.-R. and M. Schnitzer. 1997. Chemical model structures for organic matter and soils. Soil Sci. 162:115–130.

Smith, O.L. 1982. Soil microbiology: a model of decomposition and nutrient cycling. CRC Press, Boca Raton, FL, 273 p.

Smith, F.W. and S.C. Resh. 1999. Age-related changes in production and below-ground carbon allocation in *Pinus contorta* forests. For. Sci. 45: 333–341.

Song, C. and C.E. Woodcock. 2003. A regional forest ecosystem carbon budget model: impacts of forest age structure and landuse history. Ecol. Model. 164:33–47.

Trofymow, J.A., C.M. Preston and C.E. Prescott. 1995. Litter quality and its potential effect on decay rates of materials from Canadian forests. Water Air Soil Pollut. 82:215–226.

Trofymow, J.A., T.R. Moore, B. Titus et al. 2002. Rates of litter decomposition over 6 years in Canadian forests: influence of litter quality and climate. Can. J. For. Res. 32:789–804.

Tyree, M.T. and F.W. Ewers. 1991. The hydraulic architecture of trees and other woody plants. New Phytol. 119:345–360.

Waring, R.H. and S.W. Running. 1978. Sapwood water storage: its contribution to transpiration and effect upon water conductance through the stems of old-growth Douglas-fir. Plant Cell Environ. 1:131–140.

Waring, R.H. and S.W. Running. 1998. Forest ecosystems: analysis at multiple scales. 2nd Edn. Academic Press, London, 370 p.

Appendix 1: Supplementary tables presenting key equations in *ecosys* that determine forest age effects on net ecosystem productivity

Table A1. Soil organic transformations.

http://www.heronpublishing.com/tree/supplementary/Grant/Grant.Table_A1.pdf

Table A2. Plant water relations.

http://www.heronpublishing.com/tree/supplementary/Grant/Grant.Table_A2.pdf

Table A3. Gross primary productivity and autotrophic respiration.

http://www.heronpublishing.com/tree/supplementary/Grant/Grant.Table_A3.pdf

Table A4. Definition of variables.

http://www.heronpublishing.com/tree/supplementary/Grant/Grant.Definitions.pdf